Astronomy & Astrophysics manuscript no. A_A_paper
December 7, 2023

Observational study of intermittent solar jets: p-mode modulation

Qiuzhuo Cai[1], Guiping Ruan[1], Chenxi Zheng[1], Brigitte Schmieder[2,3], Jinhan Guo[2,4], Yao Chen[1], Jiangtao Su[5], Yang Liu[1], Jihong Liu[6], and Wenda Cao[7,8]

[1] Shandong Provincial Key Laboratory of Optical Astronomy and Solar-Terrestrial Environment, and Institute of Space Sciences, Shandong University, Weihai 264209, China
e-mail: `rgp@sdu.edu.cn`
[2] Centre for Mathematical Plasma-Astrophysics, Department of Mathematics, KU Leuven, Celestijnenlaan 200B, 3001 Leuven, Belgium
[3] LESIA, Observatoire de Paris, Université PSL, CNRS, Sorbonne Université, Université de Paris, 5 place Jules Janssen, 92190 Meudon, France
[4] School of Astronomy and Space Science and Key Laboratory for Modern Astronomy and Astrophysics, Nanjing University, Nanjing 210023, China
[5] Key Laboratory of Solar Activity, National Astronomical Observatories, Chinese Academy of Sciences, Beijing 100012, China
[6] Shi Jiazhuang University, Shi Jiazhuang 050035, China
[7] Center for Solar-Terrestrial Research, New Jersey Institute of Technology, 323 Martin Luther King Blvd., Newark, NJ 07102, USA
[8] Big Bear Solar Observatory, 40386 North Shore Lane, Big Bear City, CA 92316, USA

December 7, 2023

ABSTRACT

Aims. Recurring jets are observed in the solar atmosphere, which can erupt intermittently over a long period of time. By the observation of intermittent jets, we want to understand the causes of periodic eruption characteristics.

Methods. We report intermittent jets observed by the Goode Solar Telescope (GST) with the TiO Broadband Filter Imager (BFI), the Visible Imaging Spectrometer (VIS) in H_α, and the Near-InfraRed Imaging Spectropolarimeter (NIRIS). The analysis was aided/complemented by 1400 Å and 2796 Å data from Interface Region Imaging Spectrograph (IRIS).These observational instruments allowed us to analyze the temporal characteristics of jet events. By constructing the H_α Dopplergrams, we found that the plasma is first moving upward, whereas during the second phase of the jet, the plasma is flowing back. Working with time slice diagrams, we investigated the characteristics of the dynamic of the jets.

Results. The jet continued for up to 4 hours. The time distance diagram shows that the peak of the jet has obviously periodic eruption characteristics (5 minutes) during 18:00 UT-18:50 UT. We also found periodic brightening phenomenon (5 minutes) during jets bursts in the observed bands in the Transition Region (1400 Å and 2796 Å), which may be a response to intermittent jets in the upper solar atmosphere.The time lag is 3 minutes. Evolutionary images in the TiO band revealed the horizontal movement of granulation at the location of jet. Compared to the quiet region of the Sun, we found that the footpoint of the jet is enhanced at the center of the H_α spectral line profile, with no significant changes in the line wings. This suggests the presence of prolonged heating at the footpoint of the jet. In the mixed-polarity magnetic field region of the jet, we observed magnetic flux emergence, cancellation, and shear indicating possible intermittent magnetic reconnection. That is confirmed by the nonlinear force-free field (NLFFF) model reconstructed using the magneto-friction method.

Conclusions. The multi-wavelength analysis indicates that the events we studied were triggered by magnetic reconnection caused by mixed-polarity magnetic fields. We suggest that the horizontal motion of the granulation in the photosphere drives the magnetic reconnection, which is modulated by p-mode oscillations.

Key words. Sun:activity-sunspots:magnetic fields-Sun:observation

1. Introduction

Solar jets are plasma ejection phenomena observed throughout the solar atmosphere and have been extensively studied in terms of their morphology, dynamic characteristics, and driving mechanisms since their first detection in the X-ray emission of coronal jets by the Soft X-ray Telescope aboard the Yohkoh satellite in the early 1990s (Schmieder et al. 1995; Shen et al. 2019; Raouafi et al. 2016; Shen 2021; Schmieder 2022). Jets are observed in multiple wavelengths in the solar atmosphere, appearing as bright structures in the corona and as plasma flows along magnetic field lines in the chromosphere (Tian et al. 2018; De Pontieu et al. 2021; Schmieder et al. 2022). They have been referred to as H_α surges, plasma ejections, and chromospheric jets in previous studies (Roy 1973; Asai et al. 2001; Louis et al. 2014). Recently, some researchers have also called them light walls (Yang et al. 2015) or peacock jets (Robustini et al. 2016). Zhao et al. (2022) analyzed recurrent jets that repeatedly propagated from one end to the other in the chromosphere. Many jets have been observed in sunspots, while others occur in light bridges, such as the fan-shaped jets near sunspot light bridges studied by Liu et al. (2022). The first observation of fan-shaped jets on sunspot light bridges was reported by Asai et al. (2001), who found that these jets had speeds of about 50 km/s and a maximum length of 2 mega meters, suggesting that the jets originate from emerging magnetic flux with no compelling observational evidence.

Jets can occur above neutral lines of magnetic fields (Hou et al. 2016) and are believed to be triggered by magnetic reconnection, either in combination with magnetic acoustic waves (Zhang et al. 2017), magnetic reconnection (Hou et al. 2017; Bai et al. 2019; Yang et al. 2019), or a combination of both (Tian et al. 2018; Huang et al. 2020). Magnetic reconnection is widely considered as the triggering mechanism for jets, and researchers have been searching for evidence of magnetic reconnection in the solar atmosphere. Some high-resolution observations have shown inverted Y-shaped jets occurring frequently in coronal holes and active regions around sunspots (Cirtain et al. 2007; Singh et al. 2012; Yang et al. 2011; Tian et al. 2012; Zhang & Ji 2014; Shen et al. 2012). Inverted Y-shaped jets are considered to be the result of reconnection between small-scale magnetic bipolar and unipolar background fields, providing strong evidence for magnetic reconnection (Moreno-Insertis & Galsgaard 2013; Chen et al. 2015; Tian et al. 2018). The former authors studied reconnection-driven jets occurring repeatedly on light bridges of sunspots. They examined jets that frequently occurred in the wings of the H_α line and found that many jets exhibited an inverted Y-shaped structure, demonstrating a typical reconnection process in a unipolar magnetic field environment where the overlying magnetic field of the penumbra reconnected with newly emerged magnetic flux. There is also a wealth of evidence from numerical simulations that supports the connection between jets and magnetic reconnection. For example, Yokoyama & Shibata (1995, 1996) performed numerical simulations based on the magnetic reconnection model to reproduce coronal X-ray jets, which successfully demonstrated the connection between jets and magnetic reconnection. They generated anemone jets and bidirectional jets in their simulations based on two different initial magnetic field configurations. The anemone jets were produced by reconnection between newly emerged and coronal sheared fields, mostly along the spine (Joshi et al. 2020; Zhu et al. 2023). The bidirectional jets were produced by reconnection between newly emerged and overlying fields (Ruan et al. 2019). Both types of jets confirmed the occurrence of magnetic reconnection.

It is generally believed that jets are associated with the emergence and cancellation of magnetic flux. Many observational results support the model of magnetic reconnection triggering jet events. The interaction between emerging magnetic flux fields and the mobile magnetic structure can trigger jet events (Brooks et al. 2007). Kurokawa & Kawai (1993) found that jets were frequently observed and recurred for several hours, leading to the conclusion that magnetic reconnection between the newly emerged flux and pre-existing magnetic fields is the basic mechanism for generating jets. Shimojo et al. (1998) studied the magnetic field characteristics of X-ray jets and found that jets occur in unipolar, bipolar, and mixed-polarity regions, highlighting the importance of the magnetic field environment in the occurrence of jets. Chae et al. (1999) analyzed transition region ultraviolet jets and found that they repeatedly occur in regions where pre-existing magnetic flux of opposite polarity cancels out with newly emerged magnetic flux. Liu & Kurokawa (2004) studied a jet event in an emerging flux region and found a close correlation between the jet and the newly emerged bipolar structure, suggesting that an enhanced magnetic cancellation process triggered the jet. Yoshimura et al. (2003) reported a close correlation between jet at the edge of emerging flux regions, magnetic cancellation, and ultraviolet brightening, indicating a strong spatiotemporal relationship between jets and the brightening observed in the photosphere, especially during the early stages of flux emergence, which is consistent with the model of magnetic reconnection.

In addition to the scenario of magnetic reconnection triggering jets, MHD waves in the photosphere may also play a role. Magnetic-acoustic waves caused by p-mode leakage or Alfvén waves can lead to the formation of shocks, which then propels the plasma into magnetic flux tubes by increasing the magnetic pressure of the giant spicules (Shibata 1982). Shibata (1982) used a one-dimensional MHD, model to explain why the spicules are longer in coronal holes, with the key process being the increased intensity of chromospheric shock waves. Based on this, Iijima & Yokoyama (2015) studied the influence of coronal temperature on chromospheric jets and found that jets eject further outward when the coronal temperature is lower (similar to coronal holes) through two-dimensional MHD simulations. Subsequently, Iijima & Yokoyama (2017) used a three-dimensional MHD model to study jets generated by twisted magnetic field lines and observed the excitation of various MHD waves and the generation of chromospheric jets in their simulations. The strong twisting of magnetic field lines in the chromosphere helps to drive the jets through the action of Lorentz forces, making jets a natural outcome of oscillatory motion.

Repeated jets often occur in mixed polarity regions (Chen et al. 2015; Jiang & Wang 2000; Guo et al. 2013; Joshi et al. 2017), where persistent flux emergence, cancellation, and convergence can lead to the repeated occurrence of jets. Repeating jets often occur in nearly the same location (Schmieder et al. 1995; Chifor et al. 2008; Zhang et al. 2012; Wang & Liu 2012; Wang et al. 2006). Cirtain et al. (2007) detected an average of 10 jet events per hour in a 100-hour observation and found that jets often occurred at the same X-ray bright point or very close to the location of the previous jet onset. Jiang et al. (2007) observed three jet events occurring intermittently within approximately 70 minutes. Guo et al. (2013) reported three recurring EUV jets within an hour and attributed them to repetitive accumulated currents. Mulay et al. (2017) studied periodic jets using Si IV 1400 Å data obtained from the Interface Region Imaging Spectrograph (IRIS) slit-jaw imager (SJI) and observed bright and compact plasmas, suggesting a helical motion along the apex of the jet. Yang et al. (2015) discovered many bright structures rooted in active region sunspot light bridges and named them "light walls." The tops of these bright walls exhibit sustained upward and downward motion, oscillating in height with a period of approximately 4 minutes. They interpreted these oscillations as leakage of p-mode waves from beneath the photosphere.

P-mode oscillations in the photosphere may contribute to periodic solar activities, as evidenced by Chandra et al. (2015), who reported recurring jets with an oscillation period of approximately 3 minutes. They suggested that the increase and decrease of the sunspot oscillation power before and after the jet can indicate the occurrence of magnetic reconnection dominated by wave, and then modulate the 3-minute period of the jet, which possibly correspond to the leakage of 3-minute slow magnetoacoustic waves. Recently 3D (3-dimensional) numerical magnetohydrodynamic (MHD) simulations of a model solar atmosphere with a uniform, vertical and cylindrically symmetric magnetic field, mimicking the behaviour of p-mode oscillations have been performed in a pore (Griffiths et al. 2023). They conclude that magnetic regions of the solar atmosphere are favourable regions for the propagation of a small leakage of energy by slow magneto-sonic modes. It was found that the oscillations are enhanced by a vertical magnetic field. The results also exhibit a variation in the frequency of the oscillations at different heights in the low-to-mid solar atmosphere and for different values of the magnetic field.

Zeng et al. (2013) found a recurring jet with a 5-minute period in their previous study. Hong et al. (2022) studied quasi-periodic micro-jets driven by granulation convection and proposed that the persistent cancellation of opposite-polarity magnetic flux triggered by p-mode oscillations from the solar interior modulates the possibly intermittent magnetic reconnection, thus controls the 5-minute periodicity of the jets. The modulation of magnetic reconnection by p-mode oscillations is more likely to occur in small-scale, low-height jet events beneath the chromosphere (Chen & Priest 2006; Hansteen et al. 2006; De Pontieu et al. 2007), and further observational evidence is expected to support this.

In this paper, we present high-resolution observations of intermittent jets obtained by the Goode Solar Telescope (GST) operating at the Big Bear Solar Observatory (BBSO), as well as by Solar Dynamic Observatory (SDO) coupled with the Helioseismic and Magnetic Imager (HMI) and the Interface Region Imaging Spectrograph (IRIS). We analyze the dynamic characteristics of the intermittent jets, the line profile and Doppler velocity at the footpoints of jets. Additionally, we analyze the transition region brightening phenomenon and the magnetic field environment of the jets studied by a NLFFF analysis in Section 2. In Section 3, we summarize our results and discuss the influence of granular motions on the triggering mechanism of intermittent jets.

2. Observations

2.1. Instruments

On August 6, 2016, intermittent jets were observed between the two main sunspots of negative polarity forming the leading part of NOAA AR 12571 located at N13W05 with the Big Bear Solar Observatory (BBSO) coupled with the 1.6 meter Goode Solar Telescope (GST) (Goode & Cao 2012) as well as the Solar Dynamic Observatory (SDO) (**?**) coupled with the Helioseismic and Magnetic Imager (HMI) (Scherrer et al. 2012; Schou et al. 2012) and the Interface Region Imaging Spectrograph (IRIS) (De Pontieu et al. 2014). The pointer of the GST was centered on the eastern sunspot in the leading polarity of the active region.

The GST data contain simultaneous observations of the photosphere, using the titanium oxide (TiO) line taken with the Broadband Filter Imager, and the chromosphere, using the H_α 6563 Å line obtained with the Visible Imaging Spectrometer (VIS) (Cao et al. 2010). The passband of the TiO filter is 10 Å, centred at 705.7 nm, while its temporal resolution is about 15 s with a pixel scale of $0.''034$. Concerning the VIS, a combination of 5 Å interference filter and a Fabry-Pérot étalon is used to get a bandpass of 0.07 Å in the H_α line. The VIS field of view (FOV) is about $70''$ with a pixel scale of $0.''029$. To obtain more spectral information, we scan the H_α line at 5 positions with a 0.4Å step following this sequence:± 0.8, ± 0.4, 0.0 Å. We obtained a full Stokes spectroscopic polarimetry using the Fe I 1565 nm doublet over a $85''$ round FOV with the aid of a dual Fabry-Pérot etalon by the NIRIS Spectropolarimeter. Stokes I, Q, U and V profiles were obtained every 72 s with a pixel scale of $0.''081$. All TiO and H_α data were speckle reconstructed using the Kiepenheuer-Institute Speckle Interfer-ometry Package (Wöger et al. 2008).

We analyze firstly the vector magnetic field, and continuum intensity data given by HMI. Generally, HMI provides four main types of data: dopplergrams (maps of solar surface velocity), continuum filtergrams (broad-wavelength photographs of the solar photosphere), and both line-of-sight and vector magnetograms (maps of the photospheric magnetic field). The processed HMI continuum intensities and magnetograms data are obtained with a 45 s cadence and a $0.''6$ pixel size, provided by the HMI team. For comparison with NIRIS we analyzed the HMI magnetograms in the 24 hours before the event. Continuum intensity maps of HMI help us to co-align the TiO, H_α images and the magnetograms taken by GST. The GST images taken at each wavelength position were internally aligned using the cross-correlation technique provided by the BBSO programmers.

IRIS provides ultraviolet images focused on the three main channels of the IRIS telescope and their corresponding wavelengths are: Far Ultraviolet Short (FUVS, 1331.56Å–1358.40Å), Far Ultraviolet Long (FUVL, 1390.00Å–1406.79Å), and Near Ultraviolet (NUV, 2782.56Å–2833.89Å). Wideband filters in CCD imaging provide the imaging data for the Slit-Jaw Imager (SJI). IRIS observed in the sit-and-stare spectral mode with one slit located just at the North edge of the eastern leading sunspot, just in the middle of the FOV of GST. In this study, we used image from the SJI channels at 2832Å, 2796Å, and 1400 Å and the Si IV spectra (see section 3). The co-alignment between HMI continuum and GST/IRIS images was achieved by comparing commonly observed features of sunspots in Fe I 6173Å images and TiO, H_α ± 0.8Å images taken frame by frame.

2.2. Intermittent jets

In the present work, we are interested in intermittent jets in the leading spot of AR 12571 observed in the H_α lines with the GST. According to the sunspot whorls, the helicity of the active region is positive. The event occurs between 17:50:53 UT and 21:40:16UT, lasting for a duration of 4 hours. Figure 1 shows the temporal evolution of the event for three wavelengths: TiO, H_α -0.8 Å and H_α+ 0.8 Å at four different times, indicating the occurrence of jets throughout nearly 4 hours observation. From the H_α blue wing (-0.8 Å) images, it is evident that the jets predominantly erupted from the right side of the observed spot. The evolution of images in the TiO show compression motion in the granulation at the jet location, which may trigger magnetic reconnection.

Using the observation data from the H_α blue wing (-0.8 Å), we selected the red curve shown in Figure 2 (a) as the slice position (referred to as S1) and obtained a time-distance diagram of the jet eruption from 17:59:25 UT to 19:58:32 UT (Figure 2(b)). It can be observed that the jet continuously erupted with varying height. Interestingly, between 18:00:00 UT and 18:50:00 UT, the time-distance diagram of the jets shows certain periodicity. In Figure 2(b), we marked the peak time of jet eruption height with green vertical lines, and it was found that the jet erupted approximately every 5 minutes during this period. This periodicity is likely related to the magnetic field environment in which the jet is situated.

2.3. Transition region response

To investigate the phenomena of intermittent jets in the solar atmosphere above the chromosphere, we obtained slit-jaw imaging (SJI) data from the Interface Region Imaging Spectrograph (IRIS) for three wavelengths: 2832 Å, 2796 Å and 1400 Å. The IRIS observation data cover approximately two hours from 17:59:26 UT to 19:58:41 UT. To confirm whether these bright-

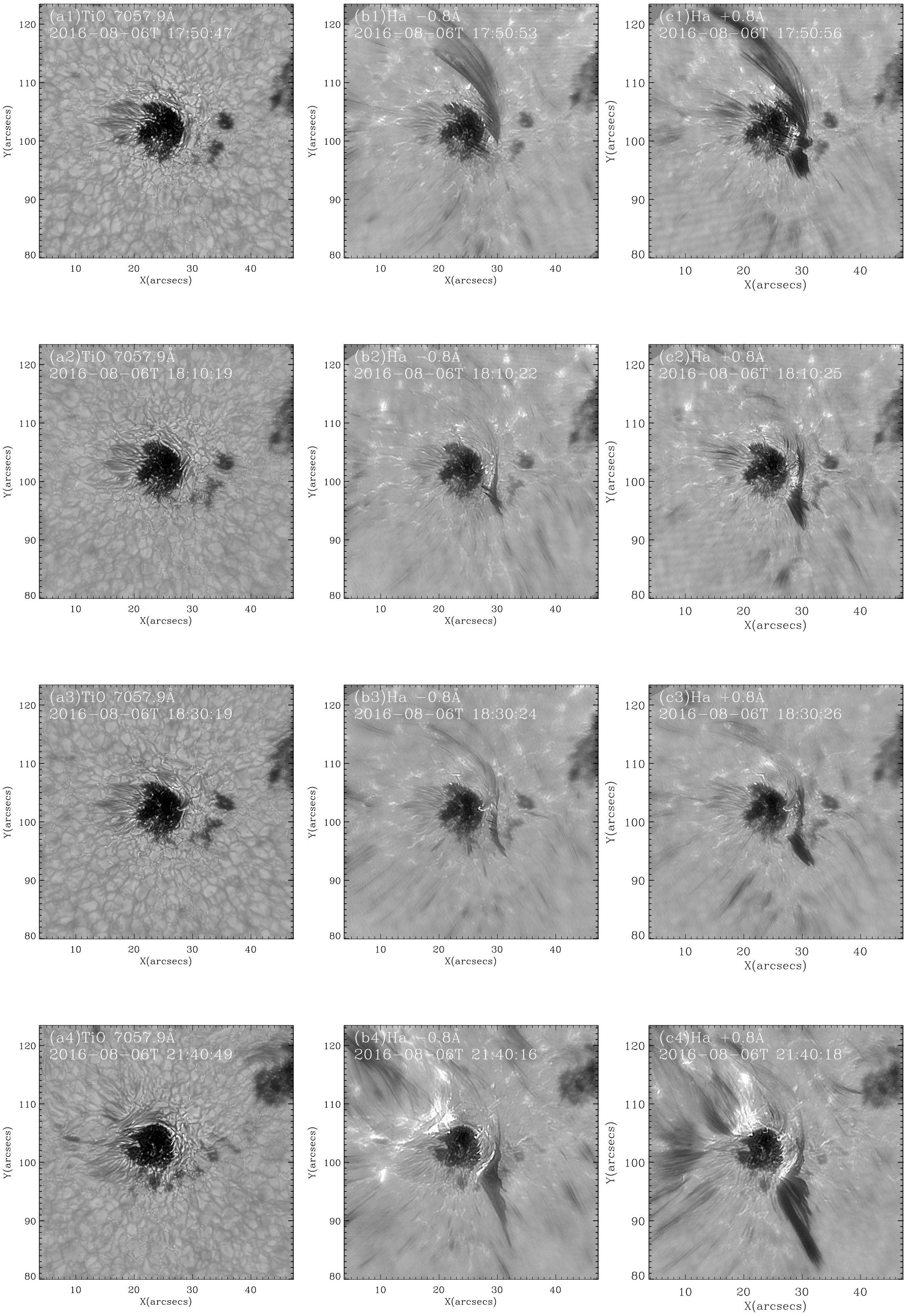

Fig. 1. Temporal evolution of intermittent jets observed in the active region NOAA 12571 with the GST at BBSO on August 6 2016 between 17:50 UT and 21:40 UT. The different panels show: the TiO images (panels a1, a2, a3, a4), the H_α blue wing images at -0.8 Å (panels b1, b2, b3, b4), and H_α red wing images at +0.8 Å (panels c1,c2, c3, c4). All Hα images are obtained with the GST/VIS.

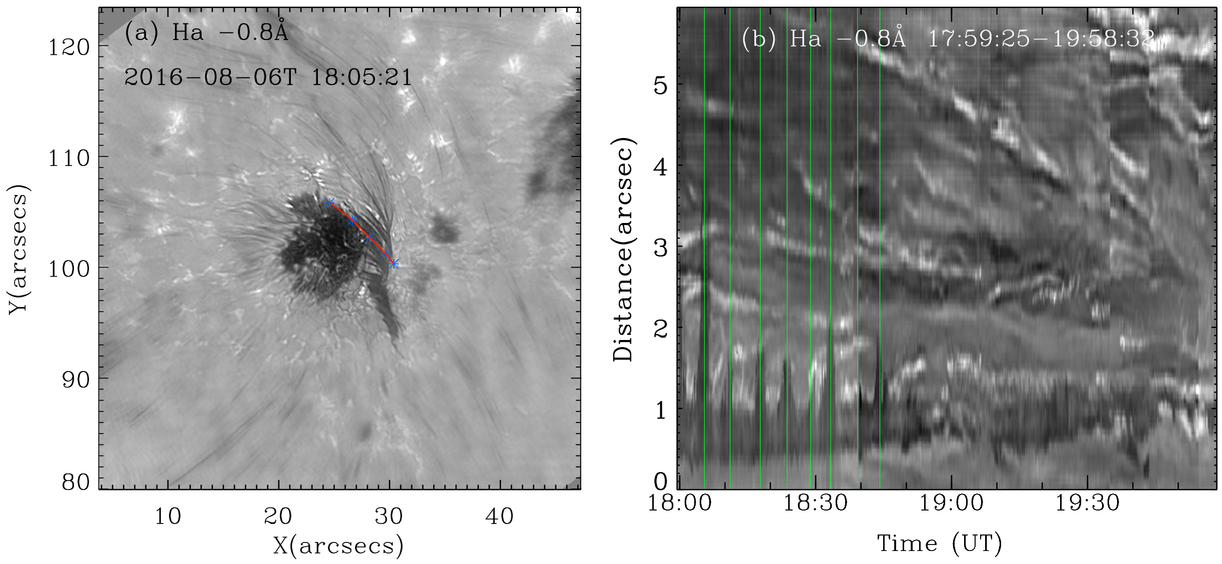

Fig. 2. Oscillation behaviour shown in the time slice diagrams in S1 (red curve) marked in the H_α blue wing image at -0.8 Å (left panel). The right panels show the plasma trajectories moving along the S1. S1 represents the motion path of the intermittent jet.

enings correspond to the intermittent jets or not, we overlaid the longitudinal magnetic field data from GST to the SJI images of the three wavelengths in Figure 3. We also identified UV brigthenings in 1400 Å and 2796 Å at the location of the jets. The brightenings precisely correspond to the boundaries of positive and negative magnetic fields, indicating the response of the intermittent jets to brightenings in the chromosphere and transition region.

To further investigate the brightening phenomena, we chose the same slice position (S1 in Figure 2) to the SJI images and plotted the time-distance diagrams in 1400 Å and 2796 Å at this slice position (see Figure 4 and Figure 5). From the two time-distance diagrams, it can be seen that the recurring brightening phenomena are presented throughout the two-hour observation period in both the 1400 Å and 2796 Å, exhibiting periodic behavior. We marked the peak time of brightenings in the time-distance diagrams with blue vertical lines and found that the brightenings in the 2796 Å and 1400 Å are consistently delayed for 2-3 minutes compared to the green vertical line in Figure 2(b). This indicates that the intermittent jets requires some time to heat up the upper solar atmosphere, and these brightening phenomena correspond to the response of intermittent jets in the lower transition region.

Regarding the IRIS observations, there are no spectral data available in this region. Additionally, we lack relevant data from SDO/AIA, so we could not obtain the response of the intermittent jets in higher solar atmosphere.

2.4. Dopplergram of the intermittent jets

In order to determine the line-of-sight (LOS) velocity of the intermittent jets material, we created Doppler diagrams of the plasma using the H_α 5 wavelength images from the GST observations. We calculated the center of weight of the H_α line profile at each pixel to estimate the Doppler shift relative to the reference line center. We averaged the entire observing FOV to obtain the reference line center (except the region where the sunspot is located) and all the line profiles were corrected by comparing them with a standard H_α profile, obtained from the NSO/Kitt Peak FTS data (Su et al. 2016).

Dopplershift maps presenting the LoS velocities are shown in Figure 6 with blue and red colors for the blue and redshift motions. It can be observed that the jet exhibits Doppler blueshift in Figure 6 (a) and Doppler redshift in Figure 6 (b). It is consistent with the observations in the H_α , which the jet displays continuous upflow and downflow over 4 hours, indicating the intermittent of the jet. We found that the average upflow speed is up to -13 km s^{-1} and the average downflow speed of the order of 11 km s^{-1} between 18:00 UT and 18:50 UT by using the shift of the central wavelength of the Hα profile. Using contrast or cloud model methods to derive the jet Dopplershifts would lead to upflows and downflows of -40 and 80 km s^{-1}, respectively.

2.5. Spectral H_α line profile

We normalized the intensity and exposure time of the H_α 5 wavelength images. It is worth noting that the reference H_α profile (averaged spectral profile of H_α on the quiet region) and the footpoint profiles are symmetric.

The corrected spectral line profile of the quiet region is used as reference to analyze the footpoint. In Figure 7 (a), we selected the footpoint $[x, y] = [617, 355]$ (yellow dot) in image of H_α +0.8 Å. The green curve is the spectral line profile of the quiet region, and the yellow curve is the spectral line profile of the footpoint. It can be seen that compared with the quiet region, the spectral line profile of the footpoint is elevated at the center of the H_α line, but there is no obvious change at the line wing, which may be because the footpoint is heated while the jet is mainly controlled by cold plasma so there is no obvious heating.

In Figure 7 (b), we selected the upflow $[x, y] = [637, 556]$ (blue dot)in image of H_α-0.8 Å. The green curve is the line profile of the quiet region, and the blue curve is the line profile of the

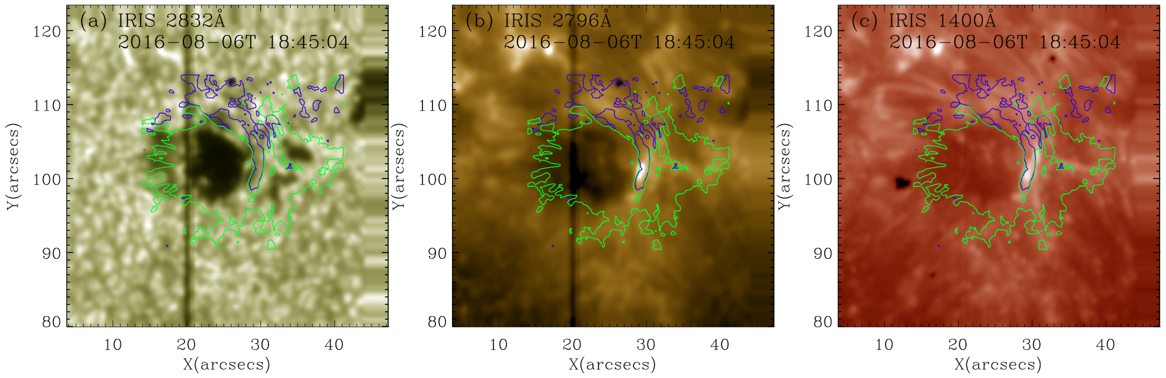

Fig. 3. The observed images of SJI 2832 Å, 2796 Å and 1400 Å superimposed by BBSO/NIRIS longitudinal field data. The blue and green lines represent the longitudinal magnetic field boundary contours of +30 and -200 G, respectively.

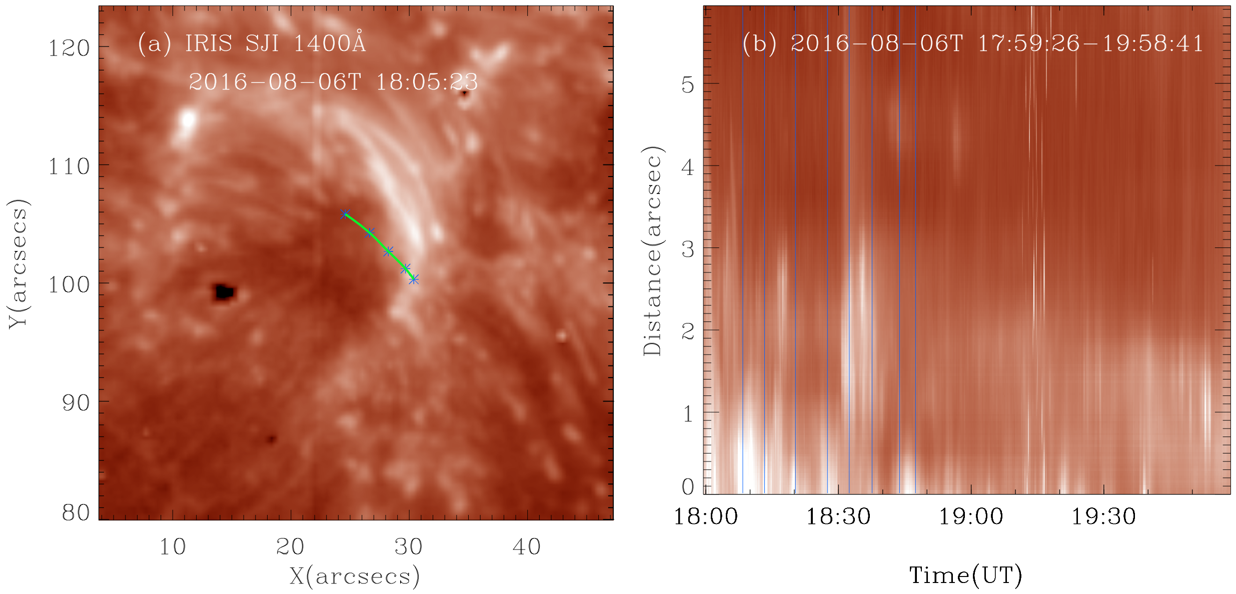

Fig. 4. Oscillation behaviour shown in the time-slice diagram of the evolution of the intensity at the jet base; (a) IRIS SJI 1400 Å image. The green curve indicates the location of the slit to make the time-slice diagram. (b) time-slice diagram along the slit. The blue vertical lines were used to mark the moments of obvious brightening.

upflow. It can be seen that the spectral line profile of the jet in the process of eruption is blue shifts , the direction of the eruption is towards the observer. In Figure 7 (c), we selected the position of the downflow $[x, y] = [704, 477]$ (red dot) in image of H_α +0.8 Å. It can be seen that the spectral line profile of downflow is red shifts, the falling direction is away from the observer.

Using SDO/HMI Sharp cea vector magnetogram data, we overlay the transverse field as arrows on the longitudinal field image to visualize the overall magnetic field information. In Figure 8(a), it can be seen that the negative polarity magnetic field converges inward, while the positive polarity magnetic field diverges outward, consistent with the direction of the positive and negative magnetic field lines. Additionally, in the regions where positive and negative magnetic fields intersect indicated by the near-parallel red and blue arrows, the magnetic field could imply a shearing behavior. This may provide the conditions for magnetic reconnection (see the area inserted in the purple contour in panel (a)). Figure 8(b) shows the NIRIS vector magnetogram of the sunspot at the time of 18:00:24 UT obtained by applying the Milne Eddington (ME) inversion to the Stokes profiles of FeI 1565 nm doublet using the inversion code of J. Chae (Degl'Innocenti 1992). The azimuth component of the inverted vector magnetic field was processed to remove the 180° ambiguity (Leka et al. 2009). We can observe the more detailed magnetic field structure which consistent with the SDO/HMI vector magnetogram observations.

Using the data from BBSO's four Stokes components, Figure 9 (a) shows the image of the longitudinal field. The spot in the center of the field of view is a negative magnetic field, and there is a positive magnetic field in the middle of spot. The jet occurs in the mixed polar magnetic field region. It may indicate the occurrence of magnetic flux emergence, magnetic cancellation and so on. In order to better determine the magnetic field environment of the jet, the high-resolution BBSO longitudinal magnetic field data is superimposed on the H_α-0.8 Å image. In Figure 9 (b), it can be seen that the footpoint is the junction of positive and negative magnetic fields, near the magnetic neutral

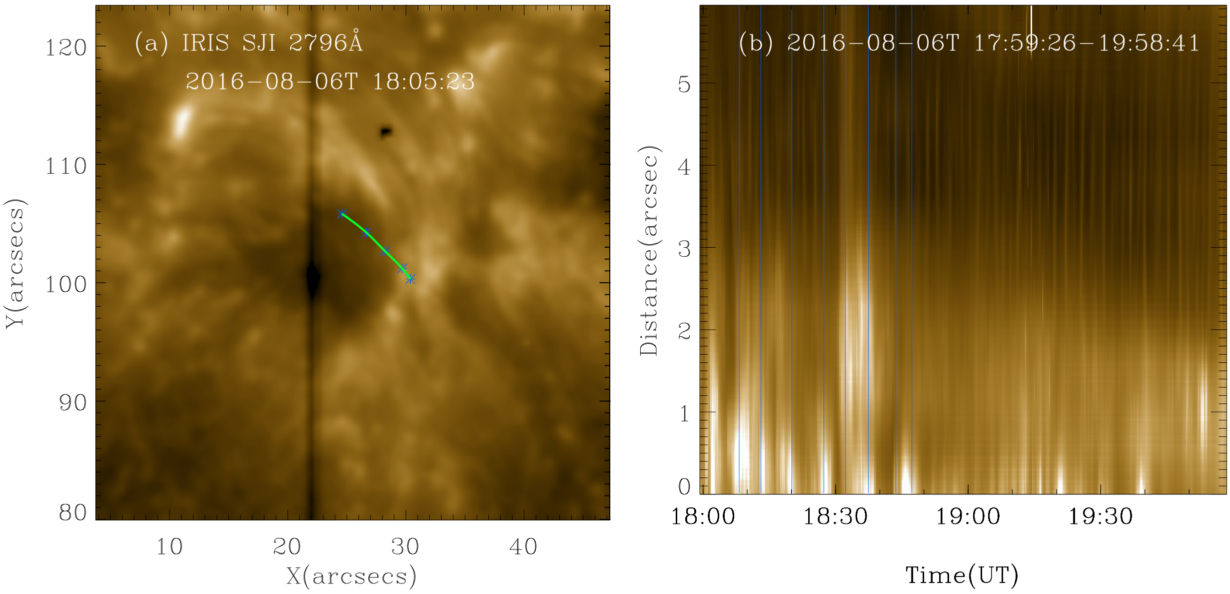

Fig. 5. Oscillation behaviour shown in the time-slice diagram of the evolution of the intensity at the jet base; (a) IRIS SJI 2796 Å image. The green curve indicates the location of the slit to make the time-slice diagram. (b) time-slice diagram along the slit. The blue vertical lines were used to mark the moments of obvious brightening.

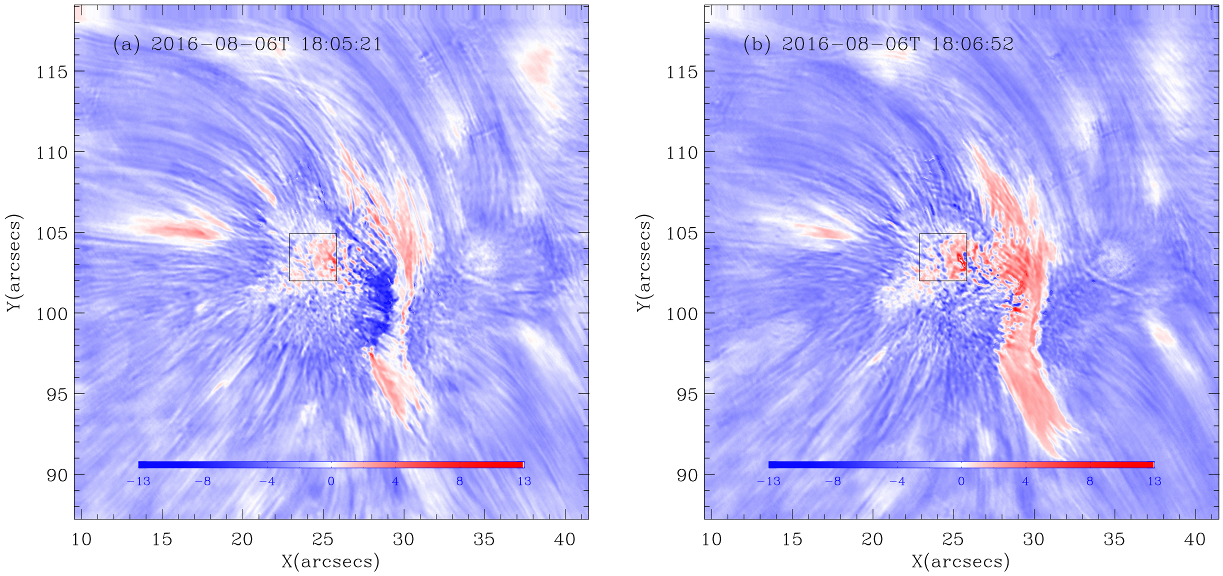

Fig. 6. LOS Doppler velocity maps obtained from GST/VIS. The black box is the subtracted reference region. The two moments represent different patterns of eruption and fall back of intermittent jets.

line. Compared with IRIS observations (see Figure 3), we found that the jet corresponds to the brightening phenomenon.

In Figure 10, using the longitudinal field data of hmi.M_45s, we selected two boundary values of positive and negative magnetic fields to determine the evolution region, then the magnetic flux is calculated. In Figure 11, it can be seen that the positive magnetic flux keeps increasing, which corresponds to the emergence of a positive magnetic field, while the negative magnetic flux first increases and then decreases, which may imply the cancellation of positive and negative magnetic fields. The emergence and cancellation of positive and negative magnetic fields may result in parallel and opposite-polarity magnetic field components, which may trigger magnetic field reconnection. It maybe trigger the intermittent jet.

2.6. The movement of granulation

In the evolution images of TiO band, we found that there is extrusion movement of granulation in the right of the spot. The local correlation tracking (LCT) method was used to superimpose the horizontal flow velocity of the photosphere to the TiO image to show the motion of granulation.

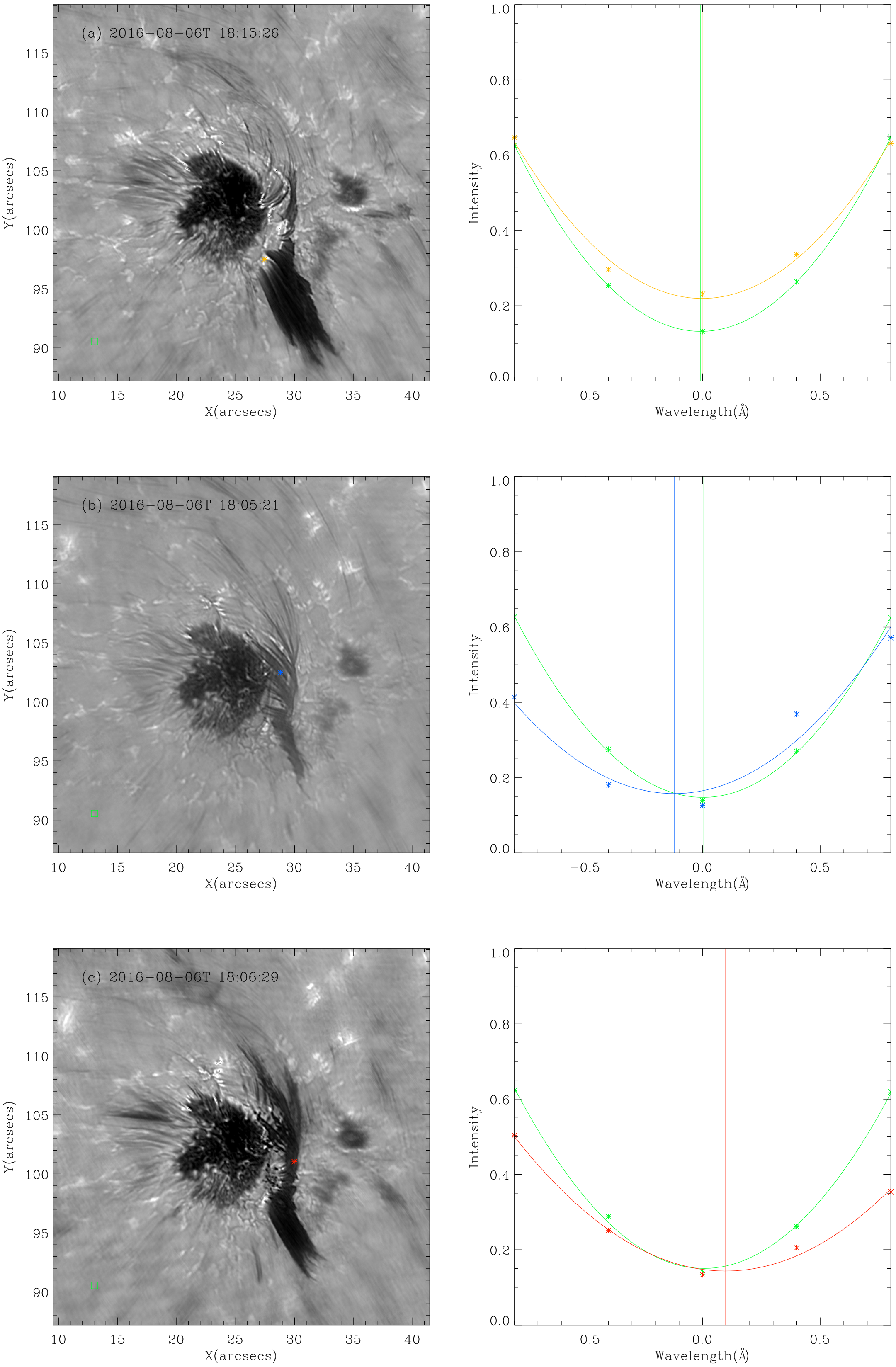

Fig. 7. Examples of normalized H_α spectral profiles in the jet and its footpoint (right panels). The top right panel corresponds to the profiles of the jet footpoint at 18:15:26 UT. Normalized H_α spectral profile (yellow line) at the footpoint of the jet and reference profile (green line) are shown in the right panel. The footpoint (yellow dot) and the quiet region (green box) are marked in image of the H_α +0.8 Å in panel (a). In panels (b) and (c) upflow (blue dot) and downflow (red dot) of intermittent jets are marked in the images of H_α +0.8 Å at 18:05 UT and at 18:06 UT respectively. Normalized H_α spectral profile of upflow (blue line), downflow (red line) and reference profile (green line) are shown in the corresponding right panels.

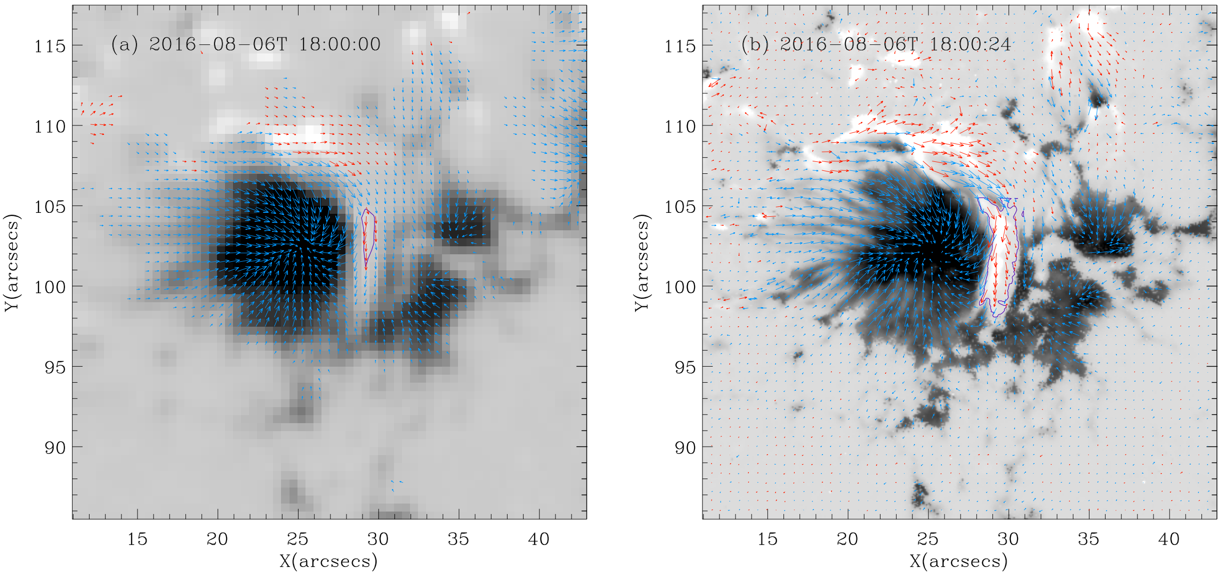

Fig. 8. (a) Vector magnetogram of the FOV obtained from SDO/HMI. The vertical component of vector magnetic field Bz in grey scale is overlaid with arrows. The red and blue arrows respectively represent the strength and direction of positive and negative transverse fields.The purple contour indicates a boundary where the longitudinal field value is 0. The area is an important location for magnetic reconnection. (b) Vector magnetogram of the FOV obtained from BBSO/NIRIS after removing the 180 ° ambiguity in the transverse field. The vertical component of vector magnetic field, B_z, in grey scale is overlaid with arrows. The red and blue arrows respectively represent the strength and direction of positive and negative transverse fields. The purple contour also indicates a boundary where the longitudinal field value is 0.

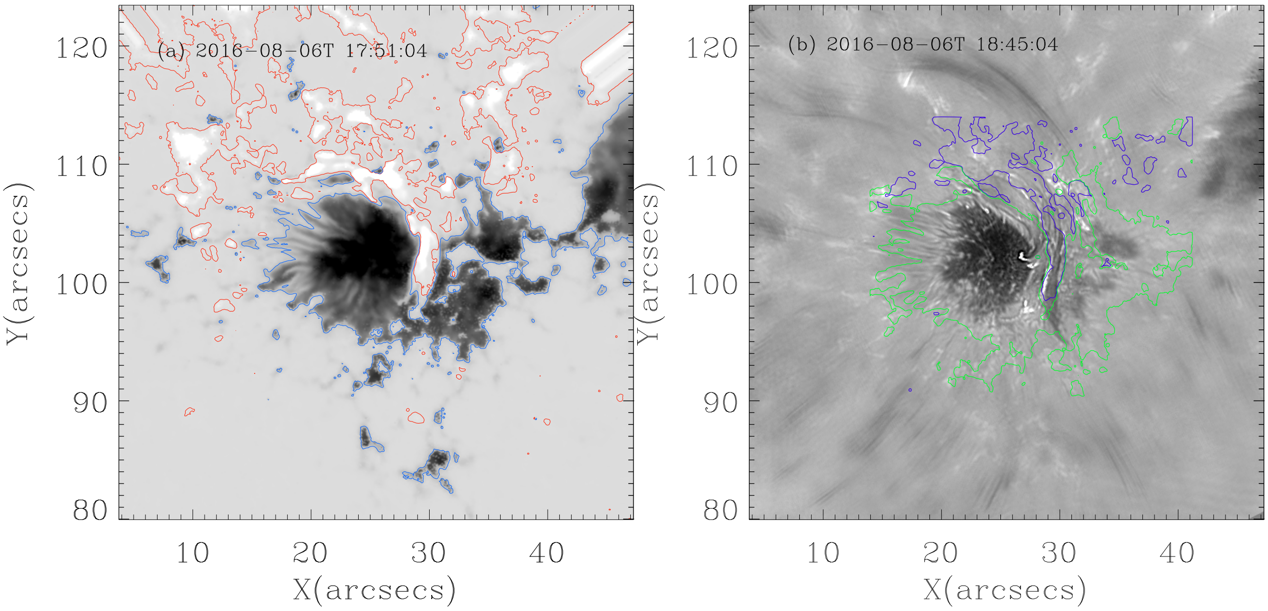

Fig. 9. (a) Longitudinal field obtained by BBSO inversion of Stokes component, the red line and blue line represent the magnetic field boundary contour of +20 G and -300 G, respectively. (b) Observation image of the H_α blue wing 0.8 Å image superimposed by BBSO longitudinal field data. The purple and green lines represent the magnetic field boundary contour of +30 and -200 G, respectively.

Figure 12 panels b and c represent the TiO emission in the area inserted in the small box drawn in panel a. This area is on the west side of the sunspot in its penumbra. In fact in this area the fibrils are not radial but turning anti-clockwise around the spot. The fibrils/magnetic field lines are anchored in the penumbra. In the panels b and c we distinguish elongated granules in this area and around it fragmented granules with filigrees in the intergranules and black pores. Horizontal components of velocity vectors are overlaid on the TiO maps. There are a few points of convergence of the arrows (in panel b point (2,2.5), and (3.5,5). They move south-west to points (in panel (c) (1,1) and (4,4). These locations move continuously away of the spot versus time as the area of the elongated granules extend toward the quiet sun. This continuous motion could be favourable for cancelling flux. The periodicity of the brightenings around 5 minutes measured in this region (Figures 2, 4, 5) would be due to the p-mode

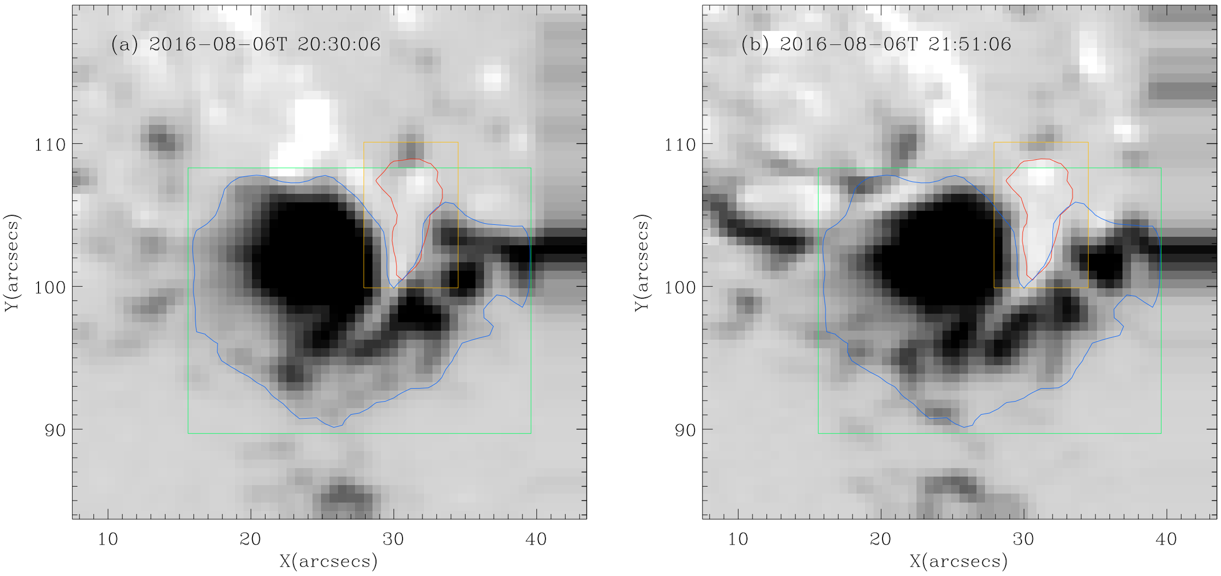

Fig. 10. Observation image of HMI M45s longitudinal field. The region surrounded by red lines in (a) and (b) is positively polar magnetic field evolution region 1 determined by the magnetic field value at 20:30:06 UT of +25 Gauss, while the blue line is negatively polar magnetic field evolution region 2 determined by the magnetic field value at 21:51:16 UT of -120 Gauss. The yellow box and the green box respectively represent the rectangular region where the positive/negative magnetic field evolution region is located.

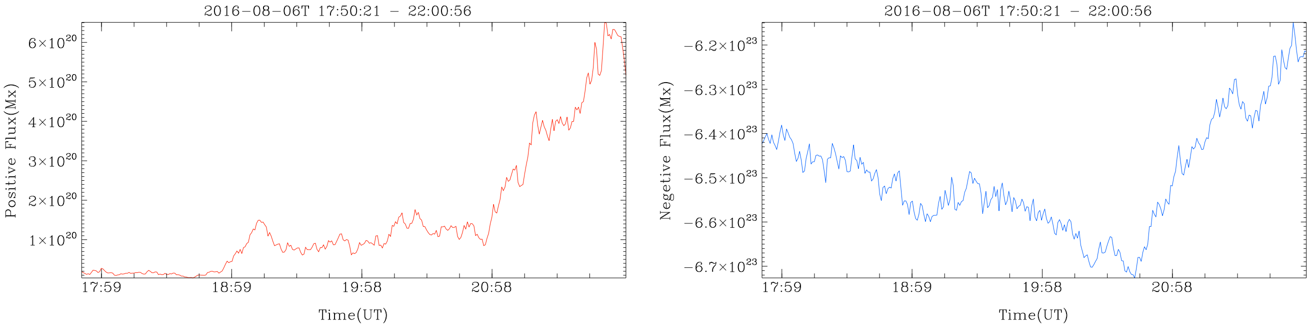

Fig. 11. Time evolution diagram of positive magnetic flux and negative magnetic flux during intermittent jet event. The red line represents the positive magnetic flux and blue line represents the negative magnetic flux.

oscillations of the photosphere modulating the radiation of this region.

3. Three-dimensional magnetic field modeling

To identify the magnetic structure of these intermittent jets, we reconstruct the 3D magnetic fields with the non-linear-force-free-field (NLFFF) extrapolation. The NLFFF extrapolation is carried out by the magneto-frictional (MF) method (Guo et al. 2016b,a) implemented in the framework of MPI-AMRVAC (Xia et al. 2018; Keppens et al. 2020, 2023). The magneto-frictional model simplifies the MHD relaxation process by omitting the effects of inertia, gravity, and pressure gradients, with velocity assumed to be proportional to the local Lorentz force. Consequently, the magnetic field evolution is governed by the magnetic induction equation, and the relaxed state approaches a force-free state (Yang et al. 1986). More details regarding the implementation and numerical schemes of the magneto-frictional model in AMRVAC framework can be found in Guo et al. (2016a,b).

We adopt the vector magnetogram (hmi.B_720s) at 18:24 UT observed by the SDO/HMI to reconstruct the coronal magnetic field. To ensure that the observed vector magnetic fields in the photosphere adhere to the assumptions of the boundary condition of the NLFFF model, we perform some preprocessing steps, including correcting projection effects (Guo et al. 2017) and removing the Lorentz force and torque (Wiegelmann et al. 2006). The initial magnetic field for the magneto-frictional model is derived using the Green's function method (Chiu & Hilton 1977) with the B_z component. The processed vector magnetic fields (B_x, B_y and B_z) are imposed on the inner ghost layer of the bottom boundary, and the values on the outer ghost layer are provided by zero-gradient extrapolation. After 60000 iterations of the magneto-frictional relaxation, the force-free metric (for more details, see Guo et al. (2016a)) decreases to half of the value of the initial potential field, while the electric current doubles. Figure 13 illustrates the results after 60000 iterations of the magneto-frictional relaxation.

Figures 13 (a) and 13 (b) display the top and side views of the reconstructed 3D magnetic fields, respectively. The yellow tubes represent the overlying background fields, and the remaining tubes that are highly sheared (cyan, pink and orange) delineate the topological structure related to the areas that intermit-

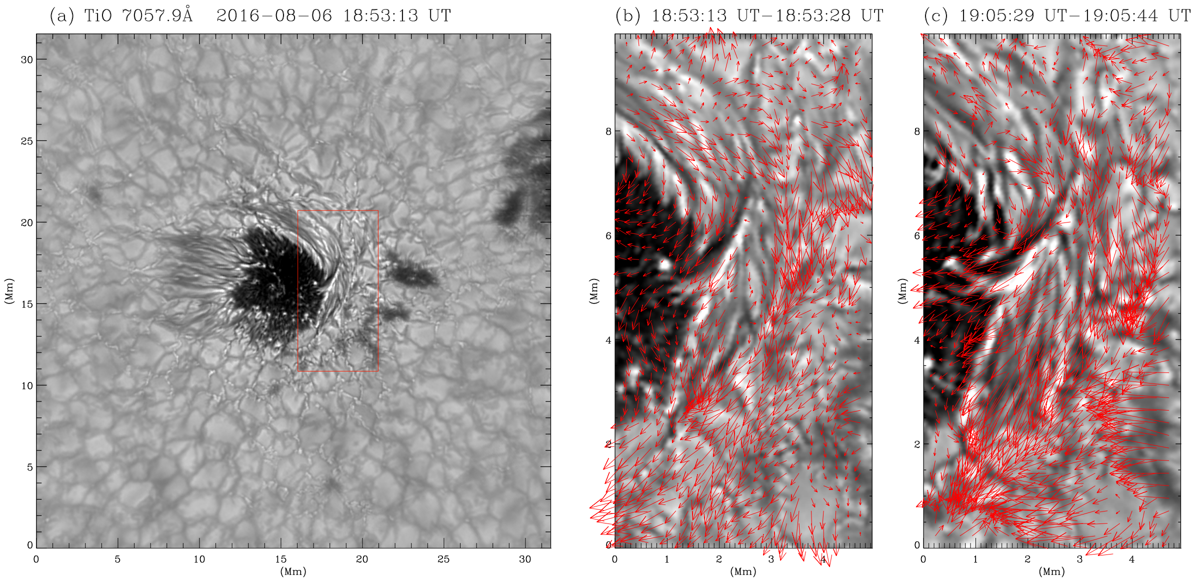

Fig. 12. Horizontal motion of granulation in the photosphere. The red arrows in (b) and (c) represents the horizontal flow of the photosphere in the red box from (a). Between 18:53 UT and 19:05 UT the whorl area around the west side of the sunspot extends toward the South-West exhibiting elongated granules with high horizontal velocity field.

tent jets take place. A good consistency can be seen between the reconstructed magnetic field lines and the observations, as highlighted in the middle panels of 13. On the one hand, the pink tubes exhibit a morphology resembling the bright structures observed by the IRIS/SJI 1400 Å. On the other hand, the cyan tubes are similar to the observed fibrils in H_α red-wing images. These results suggest that our NLFFF model almost retrieve the magnetic-field structures of the observations to a great extend.

Hereafter, to understand the underlying mechanisms resulting in the observed jets, we calculate the distribution of the squashing degree Q (Priest & Démoulin 1995; Demoulin et al. 1996) with the method proposed by Scott et al. (2017). Regions of $Q \gg 2$ depict the areas where magnetic connectivity undergoes drastic changes, commonly refereed to as Quasi-Separatrix layers (QSLs), which outline the favourite places for magnetic reconnection (Titov & Démoulin 1999; Aulanier et al. 2010; Janvier et al. 2013; Guo et al. 2013; Li et al. 2022; Zhong et al. 2021; Guo et al. 2023). Figure 13 (f) shows selected magnetic fields around the QSLs, from which one can see that cyan and orange field lines form an X-shaped configuration featured by the areas of high Q values. The reconnection between them could produce longer pink S-shaped field lines above and the green shorter loops below. A strong squashing factor (Q) value is detected at the base of the jet. This will allow for the field lines to move their direction from the North to the South and explain the southern component of the jets. For instance the yellow lines in panel (c) with South ends in high value Q factor can reconnect toward the South instead joining positive North polarities.

Figure 14 (a) illustrates the configuration of the core magnetic field of jets. It is seen that the field lines traced from the electric current channel are sheared and twisted. To quantify the degree of twist, we compute the distribution of the twist number on the same plane showing the electric current intensity, denoted as T_w, using the open-source code implemented by Liu et al. (2016). As depicted in Figure 14b, the high-T_w region forms a quasi-circular shape, corresponding to the electric current channel in Figure 14a. Furthermore, the twist number of the purple field line in Figure 14a can reach a value of 0.82, which is formed due to magnetic reconnection illustrated in Figure 13. Taken as a whole, the investigation for the 3D magnetic fields indicates that magnetic reconnection is possibly responsible for the observed jets, which is in accord with our observations.

We checked the IRIS Si IV spectra along the slit indicated in 13 (d). Two mini flares were registered at this location. During one flare at 18:33 UT we notice bilateral flows (13 (d) insert). That is indicating reconnection between the strands of the jet (Ruan et al. 2019).

4. Discussion and conclusions

In this paper, we report on coordinated observations with the GST at BBSO , SDO/HMI and IRIS SJI of the active region NOAA 12571 on August 6, 2016. The observed event shows intermittent jets occurring in the right of a negative polarity sunspot.

We obtained the following results:

1. In the H_α +/-0.8Å , we found a persistent jet in the right of the sunspot, lasting for up to 4 hours. The intermittent jets exhibited outward diverging dark absorption features.The time distance diagram shows that the peak of the jet has obvious periodic eruption characteristics (5 minutes) during 18:00 UT-18:50 UT.
2. We also observed periodic brightening in the transition region during the jets, which was reflected in the time-distance diagram. This may be a response of the intermittent jets in the higher solar atmosphere.
3. By calculating the Doppler velocities of the jets, we found alternating red shifts and blue shifts during the eruption, corresponding to the intermittent eruptive nature of the jets. The average velocities of the upflow and downflow are $-13.47\ \mathrm{km\,s^{-1}}$ and $11.11\ \mathrm{km\,s^{-1}}$, respectively if we consider the displacement of the central wavelength in the Hα profiles.

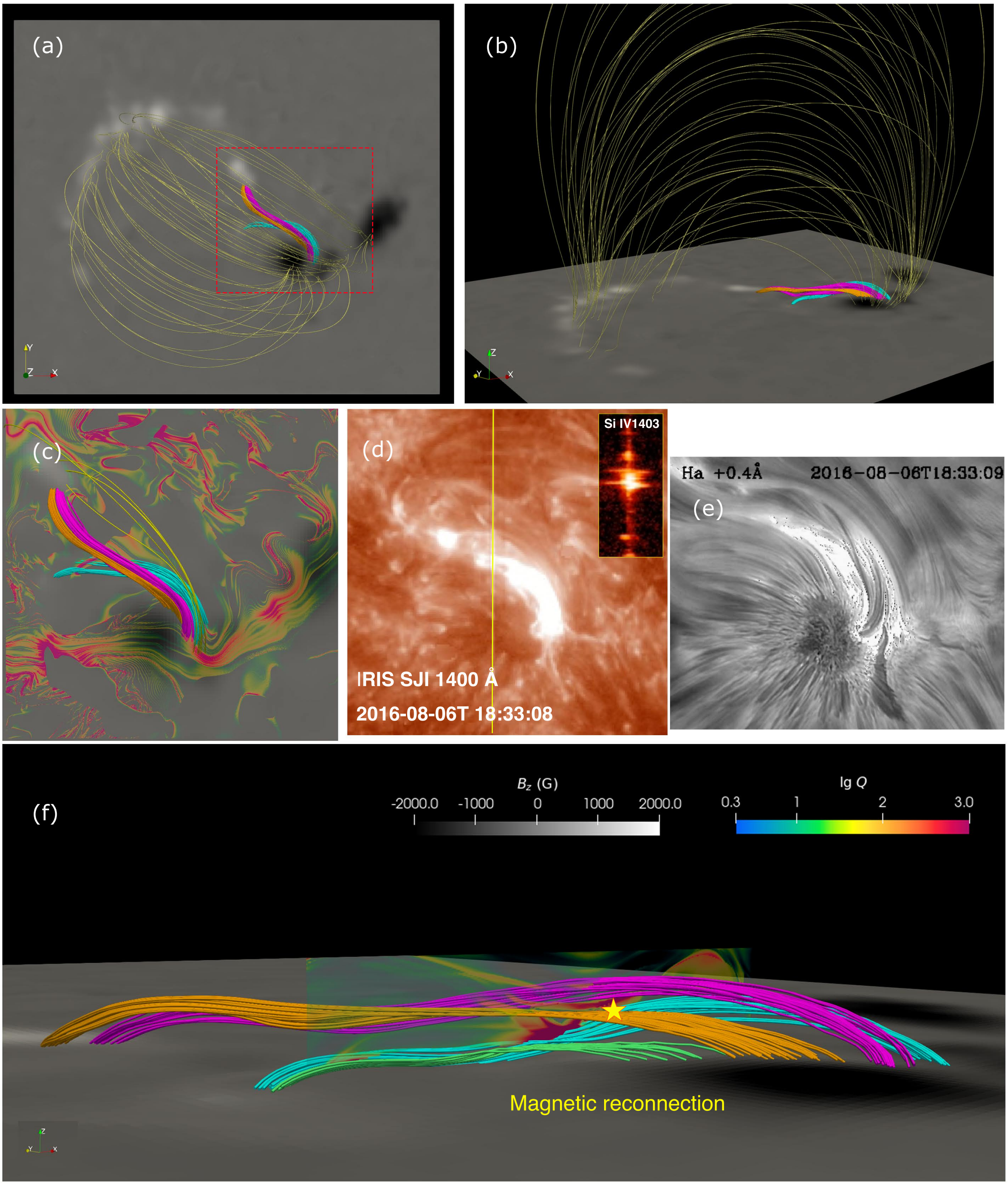

Fig. 13. 3D magnetic configuration constructed by the NLFFF model. Panels (a) and (b) exhibit the top and side views of a few typical field lines, respectively. Panels (c) presents the corresponding zoom-in view and the bottom Q distribution. Cyan and orange field lines could reconnect and lead to longer pink field lines above and short green loops below. The long yellow lines are active region magnetic field lines. Panels (d) and (e) exhibit the 1400 Å and Hα-0.8 Å images at 18:32 UT observed by the IRIS and GST, respectively. The yellow vertical line in panel (d) represents the IRIS slit, and the inset shows the spectra of Si IV 1403 Å. Panel (f) shows the reconnection configuration and the distributions of the squashing degree Q.

4. Compared to the quiet region of the Sun, we found that the spectral line profiles at the footpoint showed an intensity increase at the line center, while no significant changes in the line wings. This indicates prolonged heating at the footpoints.
5. In the vector magnetograms of the intermittent jets, we observed strong shear behavior in the magnetic field near the

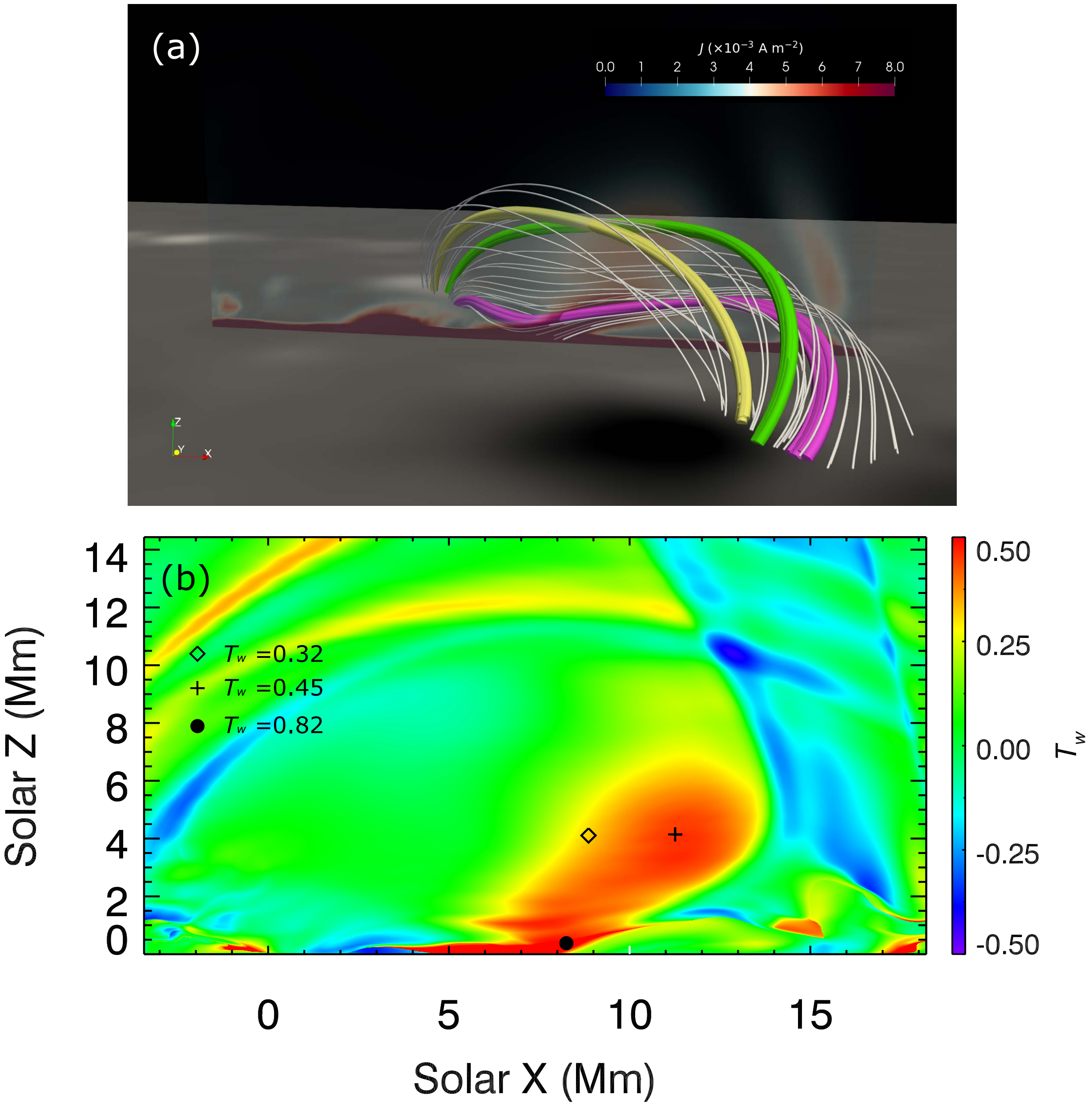

Fig. 14. Panels (a) and (b) display the typical magnetic field lines inside the electric-current channel and the twist map, respectively. The semi-transparent vertical slice in (a) shows the distribution of the electric current. The purple, green and yellow tubes in (a) are traced from the locations of the circle, plus and rhombus signs in (b), respectively.

neutral line, providing a favorable magnetic environment for magnetic reconnection.

6. By overlaying the BBSO longitudinal magnetic field onto the H_α and the IRIS SJI images in three wavelengths, we determined that the footpoints were located on the neutral line, corresponding to the brightening in the transition region and lower chromosphere. The magnetic flux evolution diagram shows that positive magnetic flux emerges continuously, and negative magnetic flux first increases and then decreases, indicating that the magnetic field has a longtime emergence and cancellation behavior.
7. The evolution image in the TiO wavelength shows horizontal motions of the granulation at the location of jets. There is intrusion of granules in this place. This may contribute to the compression of oppositely polarized magnetic fields and trigger magnetic reconnection.
8. Magneto-topology analysis for the 3D NLFFF model confirms the possibility that magnetic reconnection in the corona is the main mechanism responsible for the production of intermittent jets. It is also confirmed by spectroscopy data with bilateral flows.
9. The magnetic field lines containing the jets are anchored in the mixed magnetic polarity channel inside the negative polarity spot.

Magnetic reconnection has been widely accepted as the driving mechanism of most solar eruptive events. Many small-scale events in the solar atmosphere, such as solar jets (Asai et al. 2001; Mulay et al. 2016; Raouafi et al. 2016; Shen 2021). Many observational events can be explained by magnetic reconnection between pre-existing open magnetic field lines and newly emerging magnetic fields, and the magnetic cancellation driven by newly emerging magnetic bipoles can be regarded as slow magnetic reconnection in the lower solar atmosphere (Wang & Shi 1993; Jiang & Wang 2000). The appearance of microflares, the converging form of extreme-ultraviolet jets, and the relationship between their footpoints and annular flare brightenings all serve as evidence of magnetic reconnection in jets (Shibata 1998).

In this paper, the intermittent jet occurred in a mixed-polarity region at the boundary negative magnetic fields. By overlaying the magnetic field onto the observed images of the jets, we found that jets were located near the neutral line. The evolution of magnetic flux showed prolonged magnetic flux emergence and magnetic cancellation. This provides a favourable magnetic environment for the intermittent jets, continuously driving the ejection of plasma material. Furthermore, in the observations of the photosphere, we found horizontal motion of the granulation in the eruption area.

The relative motion between granulation and the magnetic field along the neutral line, may lead to cancellation flux, favourable for initiating jets (Tian et al. 2017; Yang et al. 2015; Li et al. 2020). The magnetic field lines could be submitted to the oscillations present in the sunspot and its environment. We have shown some evidence that magnetic reconnection could be the mechanism for triggering the intermittent jets although to confirm the temporal nature of our proposed mechanism a times series of extrapolations would be required.

Previous studies have investigated the triggering of repetitive jets by magnetic emergence and cancellation (Zhang & Ji 2014; Chae et al. 1999; Liu et al. 2016; Zeng et al. 2013), but most events lack periodicity. However, Ning et al. (2004); Doyle et al. (2006); Chandra et al. (2015) discovered repetitive eruptive events in the transition region with quasi-periodic characteristics. Wang et al. (2021, 2023) analyzed jets that also exhibited quasi-periodic features of approximately 5 minutes, and Hong et al. (2022) observed long-duration microjets that displayed quasi-periodic behavior of approximately 5 minutes. Additionally, Chen & Priest (2006) used MHD simulations to demonstrate the scenario of periodic magnetic reconnection modulated by p-mode oscillations in eruptive events.

Acknowledgements. Guiping Ruan and Qiuzhuo Cai acknowledge the support by the NNSFC grant 12173022, 11790303 and 11973031. We gratefully acknowledge the use of data from the Goode Solar Telescope (GST) of the Big Bear Solar Observatory (BBSO). BBSO operation is supported by US NSF AGS-2309939 and AGS-1821294 grants and New Jersey Institute of Technology. GST operation is partly supported by the Korea Astronomy and Space Science Institute and the Seoul National University. We thank Dr. S. Poedts for reading and bringing some fruitful comments to the manuscript. We are grateful to Shuhong Yang for the discussion on the manuscript. W. Cao acknowledges support from US NSF AST-2108235 and AGS-2309939 grants. B.S. and J.H.G. acknowledge support from the European Union's Horizon 2020 research and innovation programme under grant agreement No 870405 (EUHFORIA 2.0) and the ESA project "Heliospheric modelling techniques“ (Contract No. 4000133080/20/NL/CRS). We thank SDO/HMI, SDO/AIA teams for the free access to the data.

References

Asai, A., Ishii, T. T., & Kurokawa, H. 2001, ApJ, 555, L65

Aulanier, G., Török, T., Démoulin, P., & DeLuca, E. E. 2010, ApJ, 708, 314

Bai, X., Socas-Navarro, H., Nóbrega-Siverio, D., et al. 2019, ApJ, 870, 90

Brooks, D. H., Kurokawa, H., & Berger, T. E. 2007, ApJ, 656, 1197

Cao, W., Gorceix, N., Coulter, R., et al. 2010, Astronomische Nachrichten, 331, 636

Chae, J., Qiu, J., Wang, H., & Goode, P. R. 1999, ApJ, 513, L75

Chandra, R., Gupta, G. R., Mulay, S., & Tripathi, D. 2015, MNRAS, 446, 3741

Chen, J., Su, J., Yin, Z., et al. 2015, ApJ, 815, 71

Chen, P. F. & Priest, E. R. 2006, Sol. Phys., 238, 313

Chifor, C., Young, P. R., Isobe, H., et al. 2008, A&A, 481, L57

Chiu, Y. T. & Hilton, H. H. 1977, ApJ, 212, 873

Cirtain, J. W., Golub, L., Lundquist, L., et al. 2007, Science, 318, 1580

De Pontieu, B., Hansteen, V. H., Rouppe van der Voort, L., van Noort, M., & Carlsson, M. 2007, ApJ, 655, 624

De Pontieu, B., Polito, V., Hansteen, V., et al. 2021, Sol. Phys., 296, 84

De Pontieu, B., Title, A. M., Lemen, J. R., et al. 2014, Sol. Phys., 289, 2733

Degl'Innocenti, E. L. 1992, in Solar observations: techniques and interpretation (Cambridge University Press), 71–143

Demoulin, P., Henoux, J. C., Priest, E. R., & Mandrini, C. H. 1996, A&A, 308, 643

Doyle, J. G., Popescu, M. D., & Taroyan, Y. 2006, A&A, 446, 327

Goode, P. R. & Cao, W. 2012, in Society of Photo-Optical Instrumentation Engineers (SPIE) Conference Series, Vol. 8444, Ground-based and Airborne Telescopes IV, ed. L. M. Stepp, R. Gilmozzi, & H. J. Hall, 844403

Griffiths, M., Gyenge, N., Zheng, R., Korsós, M., & Erdélyi, R. 2023, Physics, 5, 461

Guo, J. H., Ni, Y. W., Zhong, Z., et al. 2023, ApJS, 266, 3

Guo, Y., Démoulin, P., Schmieder, B., et al. 2013, A&A, 555, A19

Guo, Y., Pariat, E., Valori, G., et al. 2017, ApJ, 840, 40

Guo, Y., Xia, C., & Keppens, R. 2016a, ApJ, 828, 83

Guo, Y., Xia, C., Keppens, R., & Valori, G. 2016b, ApJ, 828, 82

Hansteen, V. H., De Pontieu, B., Rouppe van der Voort, L., van Noort, M., & Carlsson, M. 2006, ApJ, 647, L73

Hong, Z., Wang, Y., & Ji, H. 2022, ApJ, 928, 153

Hou, Y., Zhang, J., Li, T., Yang, S., & Li, X. 2017, ApJ, 848, L9

Hou, Y. J., Li, T., Yang, S. H., & Zhang, J. 2016, A&A, 589, L7

Huang, Z., Zhang, Q., Xia, L., et al. 2020, ApJ, 897, 113

Iijima, H. & Yokoyama, T. 2015, ApJ, 812, L30

Iijima, H. & Yokoyama, T. 2017, ApJ, 848, 38

Janvier, M., Aulanier, G., Pariat, E., & Démoulin, P. 2013, A&A, 555, A77

Jiang, Y. & Wang, J. 2000, A&A, 356, 1055

Jiang, Y. C., Chen, H. D., Li, K. J., Shen, Y. D., & Yang, L. H. 2007, A&A, 469, 331

Joshi, R., Chandra, R., Schmieder, B., et al. 2020, A&A, 639, A22

Joshi, R., Schmieder, B., Chandra, R., et al. 2017, Sol. Phys., 292, 152

Keppens, R., Popescu Braileanu, B., Zhou, Y., et al. 2023, arXiv e-prints, arXiv:2303.03026

Keppens, R., Teunissen, J., Xia, C., & Porth, O. 2020, arXiv e-prints, arXiv:2004.03275

Kurokawa, H. & Kawai, G. 1993, in Astronomical Society of the Pacific Conference Series, Vol. 46, IAU Colloq. 141: The Magnetic and Velocity Fields of Solar Active Regions, ed. H. Zirin, G. Ai, & H. Wang, 507

Leka, K. D., Barnes, G., Crouch, A. D., et al. 2009, Sol. Phys., 260, 83

Li, H. T., Cheng, X., Guo, J. H., et al. 2022, A&A, 663, A127

Li, T., Hou, Y., Zhang, J., & Xiang, Y. 2020, MNRAS, 492, 2510

Liu, J., Wang, Y., Erdélyi, R., et al. 2016, ApJ, 833, 150

Liu, Y. & Kurokawa, H. 2004, ApJ, 610, 1136

Liu, Y., Ruan, G. P., Schmieder, B., et al. 2022, A&A, 667, A24

Louis, R. E., Beck, C., & Ichimoto, K. 2014, A&A, 567, A96

Moreno-Insertis, F. & Galsgaard, K. 2013, ApJ, 771, 20

Mulay, S. M., Tripathi, D., Del Zanna, G., & Mason, H. 2016, A&A, 589, A79

Ning, Z., Innes, D. E., & Solanki, S. K. 2004, A&A, 419, 1141

Priest, E. R. & Démoulin, P. 1995, J. Geophys. Res., 100, 23443

Raouafi, N. E., Patsourakos, S., Pariat, E., et al. 2016, Space Sci. Rev., 201, 1

Robustini, C., Leenaarts, J., de la Cruz Rodriguez, J., & Rouppe van der Voort, L. 2016, A&A, 590, A57

Roy, J. R. 1973, Sol. Phys., 28, 95

Ruan, G., Schmieder, B., Masson, S., et al. 2019, ApJ, 883, 52

Scherrer, P. H., Schou, J., Bush, R. I., et al. 2012, Sol. Phys., 275, 207

Schmieder, B. 2022, Frontiers in Astronomy and Space Sciences, 9, 820183

Schmieder, B., Joshi, R., & Chandra, R. 2022, Advances in Space Research, 70, 1580

Schmieder, B., Shibata, K., van Driel-Gesztelyi, L., & Freeland, S. 1995, Sol. Phys., 156, 245

Schou, J., Scherrer, P. H., Bush, R. I., et al. 2012, Solar Physics, 275, 229

Scott, R. B., Pontin, D. I., & Hornig, G. 2017, ApJ, 848, 117

Shen, Y. 2021, Proceedings of the Royal Society of London Series A, 477, 217

Shen, Y., Liu, Y., Su, J., & Deng, Y. 2012, ApJ, 745, 164

Shen, Y., Qu, Z., Yuan, D., et al. 2019, ApJ, 883, 104

Shibata, K. 1982, Sol. Phys., 81, 9

Shibata, K. 1998, in ESA Special Publication, Vol. 421, Solar Jets and Coronal Plumes, ed. T.-D. Guyenne, 137

Shimojo, M., Shibata, K., & Harvey, K. L. 1998, Sol. Phys., 178, 379

Singh, K. A. P., Isobe, H., Nishizuka, N., Nishida, K., & Shibata, K. 2012, ApJ, 759, 33

Su, J. T., Ji, K. F., Banerjee, D., et al. 2016, ApJ, 816, 30

Tian, H., McIntosh, S. W., Xia, L., He, J., & Wang, X. 2012, ApJ, 748, 106
Tian, H., Yurchyshyn, V., Peter, H., et al. 2018, ApJ, 854, 92
Tian, Z., Liu, Y., Shen, Y., et al. 2017, ApJ, 845, 94
Titov, V. S. & Démoulin, P. 1999, A&A, 351, 707
Wang, H. & Liu, C. 2012, ApJ, 760, 101
Wang, J. & Shi, Z. 1993, Sol. Phys., 143, 119
Wang, Y., Zhang, Q., Hong, Z., et al. 2023, A&A, 672, A173
Wang, Y., Zhang, Q., & Ji, H. 2021, ApJ, 913, 59
Wang, Y. M., Pick, M., & Mason, G. M. 2006, ApJ, 639, 495
Wiegelmann, T., Inhester, B., & Sakurai, T. 2006, Sol. Phys., 233, 215
Wöger, F., Von der Lühe, O., & Reardon, K. 2008, Astronomy & Astrophysics, 488, 375
Xia, C., Teunissen, J., El Mellah, I., Chané, E., & Keppens, R. 2018, ApJS, 234, 30
Yang, L.-H., Jiang, Y.-C., Yang, J.-Y., et al. 2011, Research in Astronomy and Astrophysics, 11, 1229
Yang, S., Zhang, J., Jiang, F., & Xiang, Y. 2015, ApJ, 804, L27
Yang, W. H., Sturrock, P. A., & Antiochos, S. K. 1986, ApJ, 309, 383
Yang, X., Yurchyshyn, V., Ahn, K., Penn, M., & Cao, W. 2019, ApJ, 886, 64
Yokoyama, T. & Shibata, K. 1995, Nature, 375, 42
Yokoyama, T. & Shibata, K. 1996, PASJ, 48, 353
Yoshimura, K., Kurokawa, H., Shimojo, M., & Shine, R. 2003, PASJ, 55, 313
Zeng, Z., Cao, W., & Ji, H. 2013, ApJ, 769, L33
Zhang, J., Tian, H., He, J., & Wang, L. 2017, ApJ, 838, 2
Zhang, Q. M., Chen, P. F., Guo, Y., Fang, C., & Ding, M. D. 2012, ApJ, 746, 19
Zhang, Q. M. & Ji, H. S. 2014, A&A, 567, A11
Zhao, J., Su, J., Yang, X., et al. 2022, ApJ, 932, 95
Zhong, Z., Guo, Y., & Ding, M. D. 2021, Nature Communications, 12, 2734
Zhu, J., Guo, Y., Ding, M., & Schmieder, B. 2023, ApJ, 949, 2